SLAC–PUB–5889
August 1992
(T)

# Sudakov Effects in $p\bar{p}$ Annihilation*

THOMAS HYER

*Stanford Linear Accelerator Center*

*Stanford University, Stanford, California 94309*

## ABSTRACT

We compute the amplitudes for $p\bar{p} \to \gamma\gamma$ and $p\bar{p} \to \ell\bar{\ell}$, taking into account the Sudakov suppression resulting from radiation by isolated partons. Results for the two-photon annihilation process and form factor are presented for several candidate proton distribution amplitudes. Results are also presented for the ratio $\sigma(p\bar{p} \to \gamma\gamma)/\sigma(p\bar{p} \to e^+e^-)$, which is free of experimental and theoretical normalization uncertainties. Prospects for using these results to constrain the nucleon distribution amplitude are discussed.

Submitted to *Physical Review D*

⋆ Work supported by Department of Energy contract DE–AC03–76SF00515.

## I. INTRODUCTION

Quantum Chromodynamics (QCD), the generally accepted theory of strong interactions, has resisted detailed testing due to the extreme complexity even of perturbative calculations. With the next generation of hadron colliders on the horizon, it is of pressing importance to be able reliably to separate truly new physics from QCD phenomenology; this demands a quantitative understanding of hadronic processes and of the proton structure at the amplitude level.

The most sensitive probes of the proton structure are hard exclusive processes [1]. The analysis of such processes is hindered by the large number of Feynman diagrams contributing at tree level. To date, some of the simplest exclusive processes have been analyzed at leading order [2-4] and even at one loop [5]; however, the leading-order calculations have not quantitatively accounted for the "Sudakov suppression" [6] of exclusive reactions by radiation from isolated colored partons, which can have a substantial effect on the cross section.

In this paper, we calculate the differential cross section for the process $\gamma\gamma \to p\bar{p}$, taking into account the Sudakov suppression in the manner given by Sterman, Botts and Li [7-9].

The paper is organized as follows: Sec. 2 outlines the leading-order calculation, and discusses the use of proton distribution amplitudes. Section 3 discusses the origin of the Sudakov corrections, and summarizes the method of [7] for their calculation. Section 4 outlines our computational method; in Sec. 5, we display and comment on results for four candidate distribution amplitudes [10-13], and describe the sources of theoretical uncertainty. Section 6 summarizes the computation of the proton form factor, and presents results for the same distribution amplitudes. Finally, Sec. 7 contains our conclusions and evaluates future prospects for measuring the cross sections, and the possibility of gaining information about the distribution amplitude.

## II. THE TREE-LEVEL PROCESS

To lowest order, the amplitude for a hadronic process is given by [1]:

$$\mathcal{M}^{\lambda_1\lambda_2}_{hh'} = \sum_{m,(d)} \int [\mathrm{d}x]\ [\mathrm{d}y]\ [\mathrm{d}\vec{b}]\ [\mathrm{d}\vec{b}'] \\ \times\ \phi_m(x,b,\mu)\ T_H^{m,(d)}(x,\tilde{h},b;y,\tilde{h}',b';Q,\mu)\ \phi_m(y,b',\mu)\ , \tag{1}$$

where

$[\mathrm{d}x] \equiv \mathrm{d}x_1\,\mathrm{d}x_2\,\mathrm{d}x_3\ \delta(1-\sum_i x_i)$ , and $[\mathrm{d}\vec{b}] \equiv \mathrm{d}^2b_1\,\mathrm{d}^2b_2\,\mathrm{d}^2b_3\ \delta^2(\sum_i b_i)$ ;

$m$ and $d$ are the indices of the wavefunctions and the hard-scattering Feynman diagrams, respectively;

$\lambda_{1,2}$ are the photon helicities;

$\tilde{h}$ and $\tilde{h}'$ are the parton helicities within a hadron of helicity $h$ or $h'$;

$Q = \sqrt{|q^2|}$ is the hard process 4-momentum transfer; and

$\phi_m(x,b,\mu)$ is the distribution amplitude for partons with momentum fraction $x$ and impact parameter $b$ within the $m^{\text{th}}$ wavefunction at 'separation scale' $\mu$ (the scale above which processes are deemed 'hard').

### A. Distribution amplitudes

At leading twist, only the 3-quark "valence" Fock state contributes to the scattering amplitude. The most general form of a distribution amplitude (neglecting transverse momentum) for this state is

$$\begin{aligned}|p_\uparrow\rangle = \frac{f_N}{8\sqrt{6}} \int [\mathrm{d}x]\ &\phi_1(x)\,|u_\uparrow(x_1)\ u_\downarrow(x_2)\ d_\uparrow(x_3)\rangle \\ &+ \phi_2(x)\,|u_\uparrow(x_1)\ d_\downarrow(x_2)\ u_\uparrow(x_3)\rangle \\ &+ \phi_3(x)\,|d_\uparrow(x_1)\ u_\downarrow(x_2)\ u_\uparrow(x_3)\rangle\ ,\end{aligned} \tag{2}$$

where $f_N$ is a constant with units of $\mathrm{GeV}^2$, determined by the value of the transverse wavefunction at the origin.

Note that $x_2$ is always attached to the negative-helicity quark. The $\phi_m$ are not independent; rather, we have [10]

$$\phi_3(x_1, x_2, x_3) = \phi_1(x_3, x_2, x_1) \quad \text{and} \quad \phi_2(x) = -\phi_1(x) - \phi_3(x) .$$

Although the amplitudes $\phi_m$ are known exactly [1] only in the limit $\mu \to \infty$, several estimates [10-13] based on QCD sum rules have been advanced as models for $\phi$ at $\mu^2 \simeq$ 1–2 $\mathrm{GeV}^2$; they take the form

$$\phi_m(x_1, x_2, x_3) = 120\ x_1\, x_2\, x_3\ P_m(x_1, x_2, x_3) ,$$

where $P_m(x)$ is a quadratic polynomial. In Table 1, we show the decomposition of the model polynomials $P_1(x)$ into Appell polynomials, the eigenfunctions of the distribution amplitude evolution equation [1].

**Table 1.** Model distribution amplitude coefficients.

| Evolution Eigensolutions | | | Coefficients in | | | |
|---|---|---|---|---|---|---|
| $n$ | $b_n$ | $\tilde{\phi}_n$ | CZ[10] | COZ[11] | KS[12] | GS[13] |
| 1 | $-1$ | $1$ | 1.0 | 1.0 | 1.0 | 1.0 |
| 2 | $\frac{2}{3}$ | $x_1 - x_3$ | 4.309 | 3.675 | 3.255 | 4.105 |
| 3 | $1$ | $3x_2 - 1$ | −1.923 | −1.484 | −1.295 | −2.060 |
| 4 | $\frac{5}{3}$ | $3(x_1 - x_3)^2 + x_2(5x_2 - 3)$ | 2.248 | 2.898 | 3.969 | −4.720 |
| 5 | $\frac{7}{3}$ | $(x_1 - x_3)(4x_2 - 1)$ | −1.156 | −2.205 | 0.315 | 1.667 |
| 6 | $\frac{5}{2}$ | $7x_2 - 5 + \frac{14}{3}(x_1^2 + 3x_1x_3 + x_3^2)$ | 0.019 | 1.026 | 1.026 | 9.300 |

To minimize the effect of higher-order corrections, it is desirable to set the scale $Q$ so as to avoid large logarithmic contributions. In addition to determining $q^2$ for each exchanged gluon, we must take into account the fact that the distribution amplitudes depend somewhat on the momentum transfer $Q^2$. For the eigenfunctions shown, their evolution equation becomes

$$\tilde{\phi}_n(x;Q) = \tilde{\phi}_n(x;\mu)\left(\frac{\ln\frac{Q^2}{\Lambda^2}}{\ln\frac{\mu^2}{\Lambda^2}}\right)^{-\gamma_n},$$

with $\gamma_n = (2C_B\, b_n + 3C_F/2)/\beta$ for the $b_n$ given in Table 1; here $N_C = 3$ implies $C_B = 2/3$, $C_F = 4/3$, and $\beta = 11 - (2n_f/3)$ [1]. Botts and Sterman have shown [7] that we should choose the momentum transfer scale $Q = \omega \equiv \max_j\{|\tilde{b}_j|^{-1}\}$, where $\tilde{b}_j$ are the transverse separations of the quarks in position space. Thus we can easily extract the distribution amplitude analytically for a given $b$. Note that this form for the running of the distribution amplitude takes into account the running of $f_N$ and the quark anomalous dimension [1].

### B. Hard-scattering amplitude

Following [4], we classify the Feynman diagrams according to the topology of the gluon lines, as shown in Fig. 1.

Class (g) contains 42 diagrams, from the distinct attachments of the photon lines, but the color factor is zero; classes (a)–(f) each contain 56 diagrams, and the color factor is 4/9. Thus there are 336 diagrams to be evaluated, 192 of which are nonzero.

Fermion denominators in $T_H$ are either linear in $x$ and $y$ or of the form $\bar{x}_i y_j$ or $x_i \bar{y}_j$ (throughout this work, we use $\bar{x}_i \equiv 1 - x_i$), but never proportional to $x_i y_j$; thus soft propagators are less of a problem, and we neglect fermion transverse

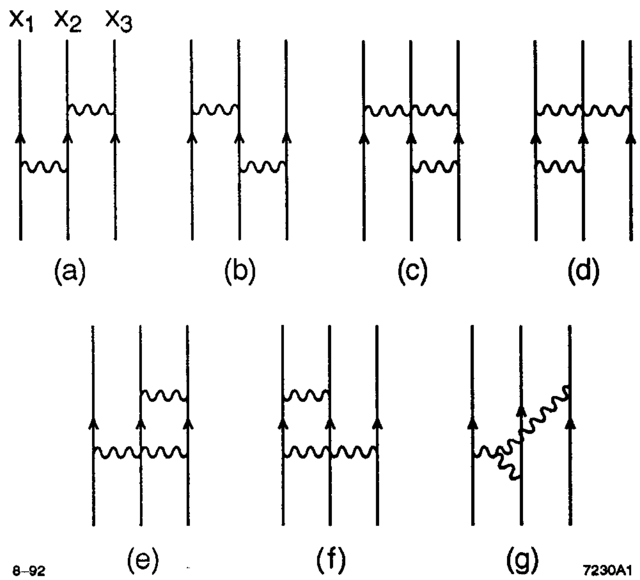


Figure 1. Classes of hard-scattering Feynman diagrams. Arrows indicate fermion flow.

momenta in $T_H^{(d)}$ [8]. Since $T_H$ now depends only on sums of the form $k_{\perp,i} + k'_{\perp,i}$, we obtain a factor in $T_H$ of $\delta^4(\vec{b} + \vec{b}')$, reflecting the heuristic notion that the $p\bar{p}$ pair is created at a point (the sign in the delta function is conventional; it arises from the fact that the $p$ and $\bar{p}$ are back-to-back).

It proves convenient to use

$$T_H^{i,(d)} = 2\delta^4(\vec{b} + \vec{b}')\, C^{(d)}\, g^4\, e_m^{(d)}\, e^2\, \tilde{G}^{(d)}\, \tilde{T}^{(d)} \ , \tag{3}$$

where $e$ and $g$ are the QED and QCD charges, and $C^{(d)}$ and $e_m^{(d)}$ are the color factor and the product of the charges of the struck quarks, respectively; then $\tilde{G}^{(d)}$ is the product of the two gluon propagators, and $\tilde{T}^{(d)}$ is a (dimensionless) kinematic quantity containing the numerator factors and Dirac propagators. To calculate $\tilde{T}^{(d)}$, we found it convenient to parametrize the photon polarization vectors by [4]

$$\epsilon_1 = \alpha\epsilon_1(\uparrow) + \beta\epsilon_1(\downarrow) , \quad \text{and} \quad \epsilon_2 = \gamma\epsilon_2(\uparrow) + \delta\epsilon_2(\downarrow) ,$$

allowing us to calculate the four photon helicity amplitudes all in one piece.

To leading twist, we may neglect quark masses so that the $u$ and $d$ quark differ only through their charge; then $\tilde{T}^{(d)}$ is flavor-independent, and the results for classes (b), (d), and (f) can be obtained from those of (a), (c), and (e), respectively, by the operation

$$\mathcal{E} : x_1 \leftrightarrow x_3 , \qquad y_1 \leftrightarrow y_3 , \qquad e_1 \leftrightarrow e_3 .$$

There is also a charge-conjugation symmetry

$$\mathcal{C} : x_i \leftrightarrow y_i , \qquad \alpha \leftrightarrow \beta , \qquad \gamma \leftrightarrow \delta , \qquad \theta \rightarrow \theta - \pi ,$$

which yields $T_H^{(\mathcal{C}d)} = \mathcal{C}(T_H^{(d)})$ for a diagram $d$; and $t \leftrightarrow u$ crossing symmetry

$$\mathcal{X} : \alpha \leftrightarrow \gamma , \qquad \beta \leftrightarrow \delta , \qquad \theta \rightarrow \theta - \pi$$

gives $T_H^{(\mathcal{X}d)} = \mathcal{X}(T_H^{(d)})$.

We calculated all diagrams in (a) and (c), and used the symmetries $\mathcal{X}$ and [in class (a)] $\mathcal{C} \circ \mathcal{E}$ to check the results. Our kinematic conventions are described in Appendix A, and the values of $\tilde{T}^{(d)}$ are tabulated in Appendix B.

We then derived the 'subamplitudes' $\tilde{T}$ for classes (b), (d), (e), and (f) by application of

$$\mathcal{E} : \text{(a)} \leftrightarrow \text{(b)} , \quad \text{(c)} \leftrightarrow \text{(d)} , \quad \text{(e)} \leftrightarrow \text{(f)} ,$$

and

$$\mathcal{C} \,:\, (\mathrm{a}) \leftrightarrow (\mathrm{b})\,, \quad (\mathrm{c}) \leftrightarrow (\mathrm{e})\,, \quad (\mathrm{d}) \leftrightarrow (\mathrm{f})\,.$$

Since we neglect the quark mass, helicity is conserved along each fermion line, and there are only eight nonzero helicity amplitudes. Because of the symmetry of the theory under $\mathcal{P}$ and $\mathcal{C}$, only two of these amplitudes are independent. We will display results for $\gamma(\uparrow)\gamma(\uparrow) \to p_+\bar{p}_+$ and $\gamma(\uparrow)\gamma(\downarrow) \to p_+\bar{p}_+$.

### C. The gluon propagator

The next problem which we face is the computation of $\tilde{G}$, the gluon propagator of Eq. (3). To avoid difficulties in convergence and retain numerical tractability, we Fourier transform [8,9] only the unrenormalized propagator from $(q_l, q_\perp)$ space to $(q_l, b_\perp)$ space.

In momentum space, the gluon denominator has the generic form

$$\frac{1}{q_l^2 - (q_\perp + l_{\perp,i} + l'_{\perp,i})^2}\,,$$

where $q_\perp$ is the portion of the hard-scattering momentum transverse to the proton momentum (see Fig. 2), and $l_{\perp,i}$, $l'_{\perp,i}$ are transverse momenta within the wavefunctions. For spacelike $q_l$, we take the Fourier transform to the hybrid $(q_l, b_\perp)$ space and average over possible orientations of $b$ to obtain

$$D_{\mathrm{space}} = -K_0\left(|b_i - b_j|\sqrt{-k^2}\,\right)\, J_0\left(|b_i - b_j||q_\perp|\right)\,,$$

where $K_0$ is a modified Bessel function and $i$, $j$ are the indices of the quark lines connected to the gluon [14,15].

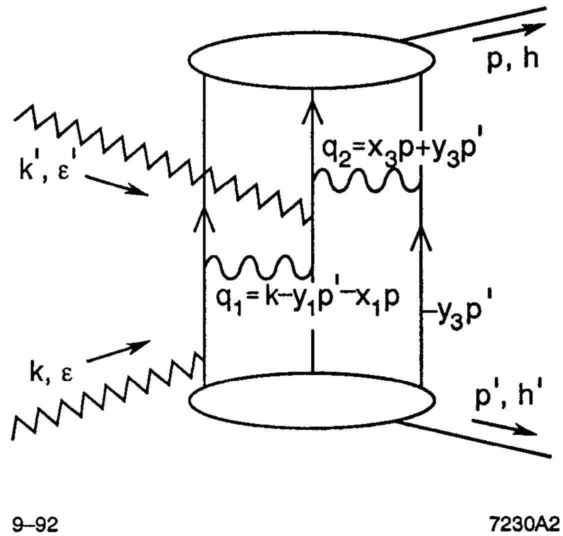


Figure 2. Diagram A24. Here $|q_{\perp,1}| = |k_\perp| = |\vec{k}| \sin\theta_{\mathrm{cm}}$, while $q_{\perp,2} = 0$.

To find the corresponding timelike propagator, we form the gluon momentum as a sum of on-shell outgoing parton momenta to obtain $(p_1 + p_2)^2 = -(p_1 - p_2)^2$; thus the timelike denominator has the same form as the spacelike denominator. Since $q_\perp \equiv 0$ for gluons of this type, we have the final form [16]

$$D_{\mathrm{time}}(q_l, b) = K_0\left(|b|\sqrt{|q_l^2|}\right) . \tag{4}$$

For the running coupling constant, we use $\alpha_s(\max\{|q_l^2|, 1/|b_\perp|^2\})$ [8]; we shall see that Sudakov suppression confines the wavefunction to $|b| < \Lambda^{-1}$, so that no further cutoff is needed. The physical justification for this choice is that very soft gluon exchange is suppressed in color singlets, so that for $b$ small the coupling does not become strong. The region in which $|b| \to \Lambda$ is strongly Sudakov suppressed, so that the divergence of the coupling there does not greatly disturb our results.

## III. SUDAKOV EFFECTS

A color singlet with zero transverse size is effectively colorless, and initial- or final-state radiation of gluons does not occur. However, the transverse size of a physical hadron cannot be neglected; for example, if in a pion the quark and antiquark are separated by a distance $b$, then gluons with transverse momentum down to $1/b$ will distinguish the pair. The sum of one-gluon corrections to the baryon valence wavefunction is proportional to

$$\frac{C_F}{\pi}\int^{Q}\frac{d^2q_\perp}{q_\perp^2}\left[3-\sum_{i<j}\exp\left\{-i(b_i-b_j)\cdot q_\perp\right\}\right]\frac{\alpha_s(q_\perp^2)}{2\pi}\int_{q_\perp}^{Q}\frac{dq_+}{q_+}\,.$$

The probability of no radiation is obtained by exponentiating this term [17], leading to the Sudakov suppression of exclusive processes for large $b$. In hadron-hadron scattering, Botts and Sterman have shown [7] that the effects of this suppression can, to leading-logarithmic order, be absorbed into the wavefunctions by the inclusion of a factor

$$\exp\left\{-\sum_i\left[s(x_iQ,\tilde{b}_i)-\int_{1/\tilde{b}_i}^{\mu}\frac{d\bar{\mu}}{\bar{\mu}}\,\gamma_q(\bar{\mu})\right]\right\}. \tag{5}$$

Here $\tilde{b}_1\equiv b_2-b_3$, etc.; $\mu$ is the separation scale, $\gamma_q$ the quark anomalous dimension, and

$$\begin{aligned}
s(\xi Q,b) = {} & \frac{A^{(1)}}{2\beta_1}\;\hat{q}\ln\left(\frac{\hat{q}}{\hat{b}}\right)+\frac{A^{(2)}}{4\beta_1^2}\left(\frac{\hat{q}}{\hat{b}}-1\right)-\frac{A^{(1)}}{2\beta_1}\;(\hat{q}-\hat{b})\\
& -\frac{A^{(1)}\beta_2}{16\beta_1^3}\;\hat{q}\left(\frac{\ln(2\hat{b})+1}{\hat{b}}-\frac{\ln(2\hat{q})+1}{\hat{q}}\right)\\
& -\left[\frac{A^{(2)}}{4\beta_1^2}-\frac{A^{(1)}}{4\beta_1}\,(2\gamma-1-\ln 2)\right]\ln\left(\frac{\hat{q}}{\hat{b}}\right)\\
& -\frac{A^{(1)}\beta_2}{32\beta_1^3}\left[\ln^2(2\hat{q})-\ln^2(2\hat{b})\right]\;,
\end{aligned}$$

where

$$\hat{q} \equiv \ln\left(\frac{\xi Q}{\Lambda\sqrt{2}}\right) , \qquad \hat{b} \equiv \ln\left(\frac{b^{-1}}{\Lambda}\right) ,$$

$$\beta_1 = \frac{33 - 2n_f}{12} , \qquad \beta_2 = \frac{153 - 19n_f}{24} ,$$

$$A^{(1)} = \frac{4}{3} , \qquad A^{(2)} = \frac{67}{9} - \frac{\pi^2}{3} - \frac{10}{27}\, n_f + \frac{8}{3}\, \beta_1(\gamma - \ln 2) ,$$

and Euler's constant $\gamma \simeq 0.577$. (Reference [8] defines $\hat{b} = +\log(b\Lambda$; our notation is otherwise identical.)

It is the result (5) which we use to model the effects of the Sudakov suppression. As in [8,9], we impose the constraint that $s(\xi Q, b) > 0$, so that the 'suppression' does not lead directly to enhancement. Also, for very small $b$ the function $s$ becomes large; in this case, we set $s = 0$ since these contributions to $s$ are from hard gluons (with momentum $\gtrsim b^{-1}$) and form a skewed subset of the higher-order hard-scattering contributions to $T_H$.

The advantage of this method is that it requires no unphysical parameters, such as a gluon mass, to retain finiteness. However, the method rests on an improved factorization obtained by retaining information about the transverse structure of the proton; thus, to implement it, we must be able to model that structure (at least in the valence state).

We can write

$$\phi_m(x, b, \mu) = \phi_m(x)\ \psi_x(b) ,$$

so that $\phi_m(x)$ is the familiar longitudinal distribution amplitude and $\psi_x(b)$ is an $x$-dependent transverse wavefunction. The definition of $\phi_m(x)$ requires the normalization [18]

$$\psi_x(\vec{b} = 0) = 1 . \tag{6}$$

The form of the noninteracting light-cone Hamiltonian [1]

$$\mathcal{H}^0_{\rm LC} \equiv P^- P^+ - \vec{P}^2_\perp = \sum_i \frac{l^2_{\perp,i}}{x_i}$$

leads us to consider a transverse wavefunction proportional to [18]

$$\exp\left\{ -\sum_i \frac{l^2_{\perp,i}}{a^2 x_i} \right\} .$$

We must determine the numerical value of $a$ in a manner consistent with its use here. We use the virial theorem. A transverse rescaling $b_\perp \to \lambda b_\perp$ affects the 'potential' (gluonic) energy of the proton by an amount parametrized by $n_U \equiv (\lambda/\langle U\rangle)\,({\rm d}\langle U\rangle/{\rm d}\lambda)$. Thus by the virial theorem, we must have

$$a^2 = \langle H^0_{\rm LC}\rangle = \frac{n_U}{2+n_U}\, m_p^2 .$$

We Fourier transform in $k_\perp$ space to obtain

$$\begin{aligned} \psi(b) = \; & \exp\left\{ -\frac{n_U m_p^2}{4(2+n_U)} \right. \\ & \left. \times \left( x_1 x_2 (b_{\perp,1} - b_{\perp,2})^2 + x_2 x_3 (b_{\perp,2} - b_{\perp,3})^2 + x_3 x_1 (b_{\perp,3} - b_{\perp,1})^2 \right) \right\} \\ = \; & \exp\left\{ -\frac{n_U m_p^2}{4(2+n_U)} \quad (x_1\, x_2\, \tilde{b}_3^2 + x_2\, x_3\, \tilde{b}_1^2 + x_3\, x_1\, \tilde{b}_2^2) \right\} . \end{aligned} \tag{7}$$

Note that $\sum_i \tilde{b}_i = 0$ and $[{\rm d}\tilde{b}] = 9\,[{\rm d}b]$.

Previous calculations [8,9] have set $n_U = 0$, neglecting the $b$-dependence of the proton wavefunction. We take $n_U = 3$ [19] for the results presented here, and use $n_U \to 0$ to examine the sensitivity of our results. At $\sqrt{s} = 5$ GeV, this substitution increases the overall normalization by 14%, and introduces variations of less than 10% for the GS model [20] and 3% for the others.

At first glance, inclusion of this transverse wavefunction appears to aggravate the divergence at small $x$, since the available volume of $b_\perp$-space increases as any $x_i \to 0$. However, the Sudakov suppression [7] contains the wavefunctions to the region where $|\tilde{b}_j| < \Lambda^{-1}$.

## IV. CALCULATIONS

Combining the results of (2–6) with (1), we obtain

$$\mathcal{M}_{hh'}^{\lambda_1\lambda_2} = \sum_m \int [\mathrm{d}x]\,\phi_m(x;\mu) \int [\mathrm{d}y]\,\phi_m(y;\mu) \int \frac{[\mathrm{d}\tilde{b}]}{9}\,\psi_x(\tilde{b})\,\psi_y(\tilde{b})$$

$$\times \exp\left\{ - \sum_j \left[ s(x_j Q, \tilde{b}_j) - \int_{\tilde{b}_j^{-1}}^{\mu} \frac{\mathrm{d}\bar{\mu}}{\bar{\mu}}\,\gamma_q(\bar{\mu}) \right] \right\}$$

$$\times \left[ \sum_{(d)} 128\pi^3\,\alpha_{\text{QED}}\,e_m^{(d)}\,C^{(d)}\,\alpha_s(q_1;\tilde{b})\,\alpha_s(q_2;\tilde{b})\,\tilde{G}^{(d)}\,\tilde{T}^{(d)}(\lambda_1,\lambda_2;h,h') \right]$$

$$\times \exp\left\{ - \sum_j \left[ s(y_j Q, \tilde{b}_j) - \int_{\tilde{b}_j^{-1}}^{\mu} \frac{\mathrm{d}\bar{\mu}}{\bar{\mu}}\,\gamma_q(\bar{\mu}) \right] \right\}. \tag{8}$$

To obtain definite predictions, we must make some simplifying assumptions. First, we replace the running coupling constant $\alpha_s(\mu^2)$ with the $n_f = 3$ form

$$\alpha_s(\mu^2) \equiv \frac{12\pi}{(33 - 2n_f)\ln\,(\mu^2/\Lambda^2)} \to \frac{4\pi}{9\ln\,(\mu^2/\Lambda^2)}\,;$$

we take $\Lambda \equiv \Lambda_{\overline{\text{MS}}}^{(3)} = 200\text{MeV}$. The range of momentum transfers which interest us runs from a few hundred MeV ($b^{-1}$ where $b$ is a typical quark impact parameter) to several GeV ($\sqrt{x_i y_i s}$, where $x_i$ and $y_i$ are typical parton momentum fractions and $\sqrt{s}$ ranges up to 7-8 GeV), which is almost exactly the region in which this approximation is viable. Certainly the resulting errors are minimal.

This form for the coupling constant allows us to rewrite (8) as

$$\mathcal{M}_{hh'}^{\lambda_1\lambda_2} = \frac{2^{12}5^2\pi^5}{3^7}\,\alpha_{QED}\,f_N^2\left(\ln\frac{\mu^2}{\Lambda^2}\right)^{4/3}$$

$$\times\sum_{m=1}^{3}\int[\mathrm{d}x]\,[\mathrm{d}y]\;x_1x_2x_3\;P_m(x)\;y_1y_2y_3\;P_m(y)$$

$$\times\int[\mathrm{d}\tilde{b}]\left[\sum_{(d)}\frac{e_m^{(d)}\;D(q_1,\tilde{b}_j)\,D(q_2,\tilde{b}_k)}{\ln\left(\max\left\{\frac{q_1^2}{\Lambda^2},\frac{1}{\tilde{b}_j^2\Lambda^2}\right\}\right)\ln\left(\max\left\{\frac{q_2^2}{\Lambda^2},\frac{1}{\tilde{b}_k^2\Lambda^2}\right\}\right)}\;\tilde{T}^{(d)}\left(\lambda_1,\lambda_2;h,h'\right)\right]$$

$$\times\prod_{i=1}^{3}\left[\frac{\exp\left\{-s(x_iQ,\tilde{b}_i)-s(y_iQ,\tilde{b}_i)-\frac{3m_p^2}{20}\left(\frac{x_1x_2x_3}{x_i}+\frac{y_1y_2y_3}{y_i}\right)\tilde{b}_i^2\right\}}{\left[-\ln(\tilde{b}_i^2\Lambda^2)\right]^{4/9}}\right],$$

where

$P_m(x)$ is a sum of Appell polynomials with weights determined by the input distribution amplitude and by $\omega\equiv\max_j\{|\tilde{b}_j|^{-1}\}$;

$e_m^{(d)}$ is the product of QED charges;

$D(q,\tilde{b})$ is the gluon propagator;

$q_1$, $q_2$ are the gluon longitudinal momenta;

$\tilde{b}_j$, $\tilde{b}_k$ are the transverse separations of the corresponding quark lines;

$\tilde{T}^{(d)}$ is the hard-scattering subamplitude of diagram $d$;

$s(xQ,b)$ is the Sudakov suppression of [7]; and

$3m_p^2/20$ is the inverse mean impact parameter for the wavefunction in our *ansatz*.

Many of the individual subamplitudes $\tilde{T}^{(d)}$ diverge as $x_i^{-1}$, and the gluon propagators diverge as $\ln(x_i)$. However, the distribution amplitude and transverse wavefunction contain factors of $x_i$, so that the integral remains convergent. To increase the numerical stability of integration, we use the change of variables

$$x_1 = \xi^2 , \qquad x_2 = \bar{x}_1 \frac{1 + \sin[\pi(\eta - 1/2)]}{2}$$

$$\Rightarrow \quad \int [\mathrm{d}x] = \int_0^1 \mathrm{d}\xi \int_0^1 \mathrm{d}\eta \;\; 2\pi\sqrt{x_1 x_2 x_3} \; ,$$

and similarly for $[\mathrm{d}y]$.

We integrated the resulting form numerically, obtaining the results shown in Figs. 3–7; in all cases, the statistical errors of the numerical integration were less than 4%, small enough to make no discernible contribution to the overall theoretical uncertainties.

## V. RESULTS AND COMMENTS

Three effects original to this paper cause our results to differ from those of its predecessors [2–3]: the Sudakov suppression itself; the consideration of the transverse wavefunction; and the running of the distribution amplitude.

The full amplitudes are shown in Fig. 3 for same-helicity photons and in Fig. 4 for opposite-helicity, with $s = 25\ \mathrm{GeV}^2$ in both cases. The same-helicity amplitude is odd in $\cos\theta_{\mathrm{cm}}$ due to crossing symmetry.

The effects of replacing the Sudakov correction with the cutoff $\alpha_s \leq 1$ are shown in Fig. 5. It is notable that for some values of $\theta_{\mathrm{cm}}$, the "suppression" actually leads to an enhancement in $\gamma_\uparrow\gamma_\downarrow \to p\bar{p}$.

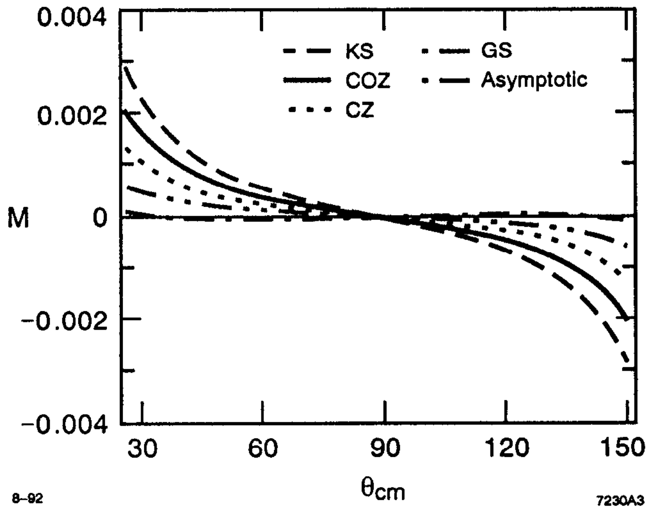


Figure 3. Amplitudes for $\gamma_\uparrow\gamma_\uparrow \rightarrow p\bar{p}$, with $s = 25\ \mathrm{GeV}^2$.

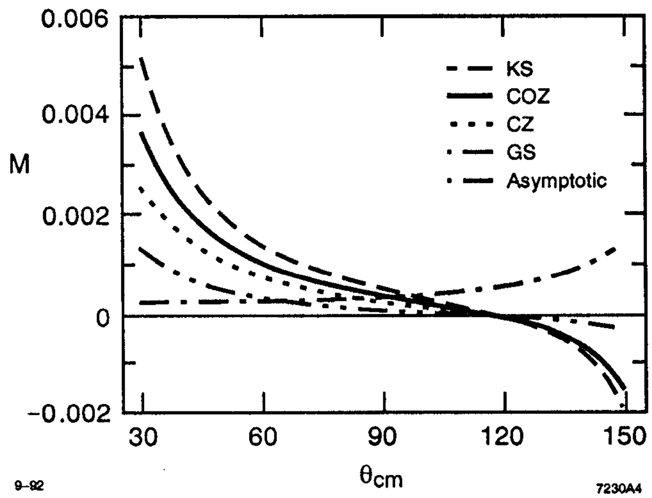


Figure 4. Amplitudes for $\gamma_\downarrow\gamma_\uparrow \rightarrow p\bar{p}$, with $s = 25\ \mathrm{GeV}^2$.

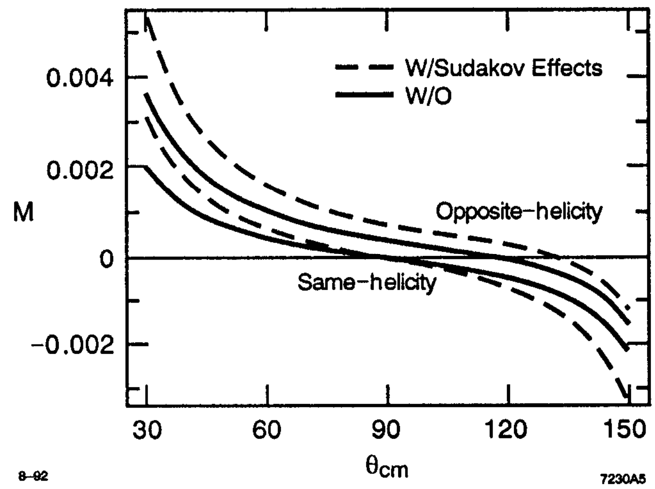


Figure 5. Effects of Sudakov suppression on $\mathcal{M}(\gamma\gamma \rightarrow p\bar{p})$, with COZ wavefunction.

Scaling of amplitudes is exhibited in Fig. 6(a) for same-helicity photons (remember that the amplitude is odd in $\cos\theta$) and in Fig. 6(b) for opposite-helicity. Both adhere closely to the dimensional-counting expectation $\sigma \propto s^{-4}$ when $s \gtrsim (5\text{ GeV})^2$; this is a sign that our method is trustworthy at these energies.

Figure 7 presents our predictions for the timelike Compton cross section. The size is quite sensitive to the choice of distribution amplitude. Recall that the cross section is proportional to $f_N^4$; $f_N$ has been determined only approximately [10] ($f_N = 5.1 \pm 0.3 \times 10^{-3}$ GeV$^2$). This uncertainty, combined with inevitable experimental normalization uncertainities, means that the total cross section alone is not a good test of the validity of a distribution. A more valid test, the shape of the cross section, is nearly the same for the three main distribution amplitudes we consider.

Note the piece of the cross section shown for the asymptotic wavefunction, which resembles none of the candidates in this energy regime.

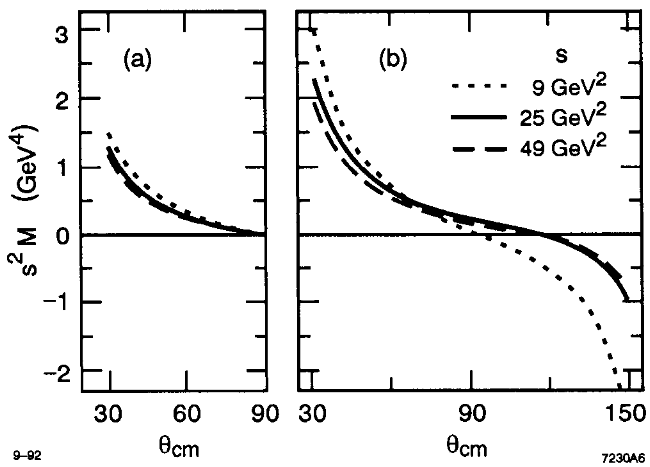


Figure 6. Violation of scaling in (a) $\gamma_\uparrow\gamma_\uparrow \to p\bar{p}$; (b) $\gamma_\downarrow\gamma_\uparrow \to p\bar{p}$, with COZ wavefunction.

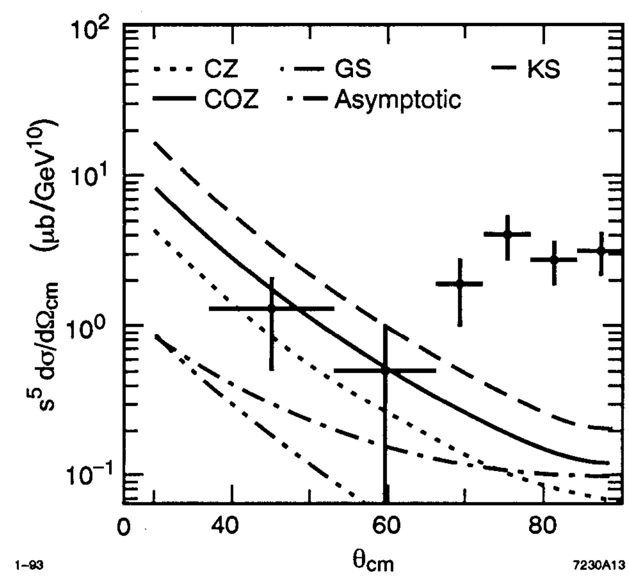


Figure 7. Normalized unpolarized differential cross section for $\gamma\gamma \to p\bar{p}$ (calculated at $s = 25\text{GeV}^2$). Data are from the JADE Collaboration, *Phys. Lett.* **174B**, 350(1986).

## VI. THE PROTON TIMELIKE FORM FACTOR

The methods discussed above can also be used to derive the timelike proton form factor

$$F_1^p(q^2 > 0) \equiv \frac{\mathcal{M}(e^+e^- \to p\bar{p})}{\mathcal{M}(e^+e^- \to \mu^+\mu^-)} .$$

In fact, the calculation of the form factor (neglecting $F_2$) offers several simplifications:

- the number of hard-scattering Feynman diagrams is greatly reduced (to 42, 28 of which vanish).
- all internal gluon momenta are timelike and purely longitudinal.
- there is no nontrivial angular or spin dependence.

The highest-energy currently available measurements of this form factor are those of FNAL E760 [21]. Figure 8 shows our predictions for the form factor and the data of [21] as a function of $q^2$. Again, the dimensional-counting rules are very accurate. Furthur experiments at FNAL E760 hopefully will extend the measurement of $F_1^p$ to higher $s$.

Figure 9 shows the dependence of the normalized form factor on a cutoff $\tilde{b} < b_{\mathrm{max}}$. Note the upward kink at $b_{\mathrm{max}} \simeq 0.9$; in this region, the one-loop running coupling $\alpha_s$ begins to grow large for small $q_l$, but the Sudakov suppression is not yet forceful. The interplay between factors contained in $\mathcal{M}$ at given $b$ is illustrated in Fig. 10, in which we have chosen for definiteness $q_1^2 = q_2^2 = 35\Lambda^2$, a typical gluonic momentum for $\sqrt{s} \simeq 5$ GeV. At small $b$, the logarithmic divergence of $K_0(bQ)$ is cancelled by the lack of phase space; as $b \to \Lambda^{-1}$, the divergence of the coupling constant is overwhelmed by the Sudakov suppression. The dominant region in our example is around $b_{\mathrm{max}} \sim 0.6\Lambda^{-1}$, while the threatening 'kink' region is just above $b_{\mathrm{max}} = 0.9\Lambda^{-1}$. In the high-energy limit, this kink will entirely disappear as the Sudakov suppression begins to force $b_{\mathrm{max}} \lesssim Q^{-1}$.

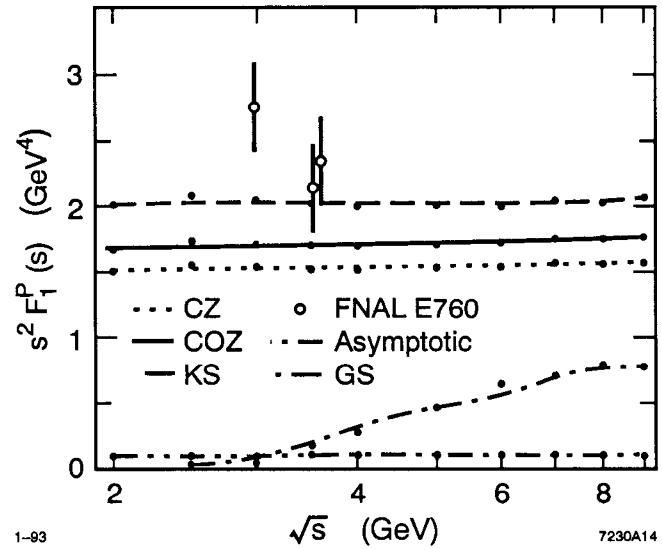


Figure 8. Normalized proton timelike form factor $q^4 F_1^p(q^2)$. Data are from Ref. [21 ].

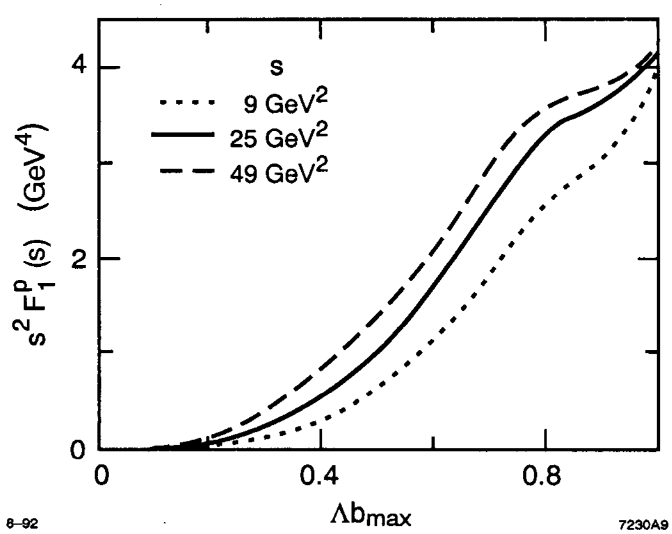


Figure 9. Accumulation of $s^2 F_1^p$ as $b_{\rm max} \equiv \max_i\{\tilde{b}_i\}$ increases, with COZ wavefunction.

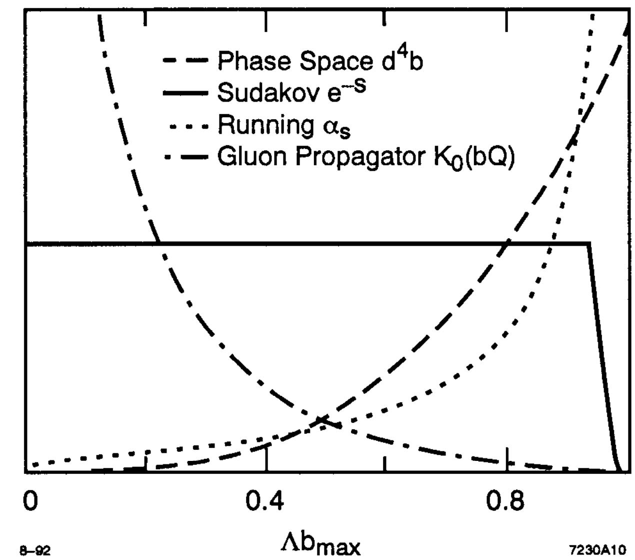


Figure 10. Factors contributing to $d\mathcal{M}/db_{\max}$.

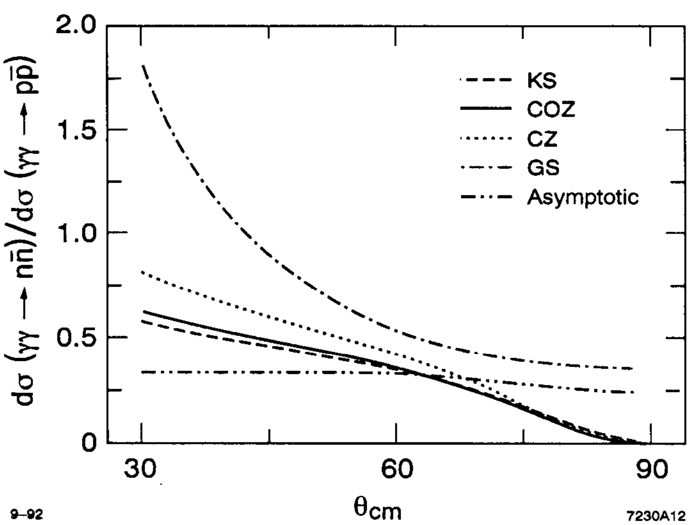


Figure 11. Ratio $d\sigma(\gamma\gamma \to n\bar{n})/d\sigma(\gamma\gamma \to p\bar{p})$ for candidate distributions at $s = 25\ \mathrm{GeV}^2$.

**Table 2.** Model distribution results for $\bar{R}_{\gamma\gamma/e^+e^-}$ and $F_1^n/F_1^p$.

| Model | CZ [10] | COZ [11] | KS [12] | GS [13] | Asymptotic |
|---|---|---|---|---|---|
| $F_1^n/F_1^p$ | 0.237 | 0.240 | 0.218 | 0.042 | 0.253 |
| $R_{\gamma\gamma/e^+e^-}$ | 5.55 | 8.9 | 12.4 | 19.1 | 200 |

The size of the 'kink contribution' is a measure of the unreliability of our results; it is about 30% at $\sqrt{s} = 3$ GeV, but decreases to 10-15% for $\sqrt{s} = 5$ GeV. This is comparable to the difference in the predictions for the COZ and CZ or KS wavefunctions; thus measurement of the form factor alone is not a powerful test of the proton distribution amplitude.

The neutron form factor $F_1^n$ and the amplitude for $\gamma\gamma \to n\bar{n}$ can be calculated in identical manner. It is unlikely that these measurements can be extended to such high energies, but proposed experiments at Frascati [21] may measure the cross section $e^+e^- \to n\bar{n}$ at $\sqrt{s} \gtrsim 3$ GeV. Thus we present here our predictions for the ratios $F_1^n/F_1^p$ (see Table 2) and $\sigma(\gamma\gamma \to n\bar{n})/\sigma(\gamma\gamma \to p\bar{p})$ (Fig. 11).

Perhaps the most interesting quantity, due to its freedom from theoretical and experimental normalization uncertainties, is the ratio

$$R_{\gamma\gamma/e^+e^-} \equiv \frac{\mathrm{d}\sigma/\mathrm{d}\Omega\,(p\bar{p} \to \gamma\gamma)}{\mathrm{d}\sigma/\mathrm{d}\Omega\,(p\bar{p} \to e^+e^-)}\ .$$

Figure 12 shows our predictions for this quantity. This ratio is much smaller for all of the candidate distributions than for the asymptotic, reflecting the strong suppression of the form factor using the asymptotic wavefunction. The values given include a correction of about 8% resulting from the running of $\alpha_{\mathrm{QED}}$.

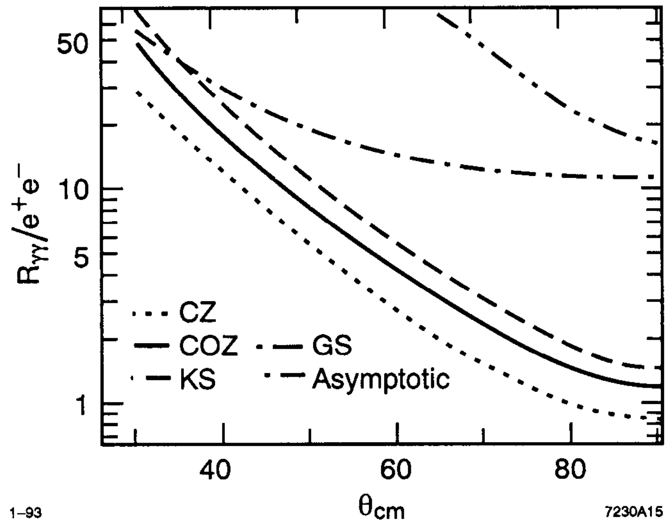


Figure 12. Ratio $R_{\gamma\gamma/e^+e^-}$ for candidate distributions at $s = 25$ GeV$^2$. Part of the curve for the asymptotic wavefunction is also shown.

The major source of model dependence in $R_{\gamma\gamma/e^+e^-}$ is the $n_U$-dependence. The results presented here were obtained with $n_U = 3$; using the flat wavefunction $n_U = 0$ decreases the predictions by 14% at $\sqrt{s} = 5$ GeV (10% at $\sqrt{s} = 7$ GeV). Certainly the flat wavefunction represents an unphysical limiting case; we maintain that this difference can be treated as a generous upper bound on the uncertainty due to variation in $n_U$.

The overall ratio

$$\bar{R}_{\gamma\gamma/e^+e^-} \equiv \frac{\sigma(p\bar{p} \to \gamma\gamma; \theta_{\rm cm} > 30^\circ)}{\sigma(p\bar{p} \to e^+e^-; \theta_{\rm cm} > 30^\circ)}$$

is displayed in Table 2 for each candidate distribution. This ratio is highly sensitive to the choice of distribution; it is also much easier to measure than either the shape of the $d\sigma/d\Omega(p\bar{p} \to \gamma\gamma)$ or the running of $Q^4 F_1^p$. Hence, it is probably one of the best tests of the proton distribution amplitude.

## VII. CONCLUSION

The value of the formalism of [7] is that it allows a consistent perturbative treatment of hadronic processes without resorting to arbitrary cutoffs. Thus the results we have just derived are (to next-to-leading log) trustworthy predictions of QCD; the size of potential errors is estimated by the magnitude of the kink contribution in the form factor, and of scaling violations in $p\bar{p} \to \gamma\gamma$. It is our belief that the model dependence of our main result, the prediction of $R_{\gamma\gamma/e^+e^-}$, is less than 15%, which is certainly adequate to allow tests of model distribution amplitudes.

High precision measurement of $R_{\gamma\gamma/e^+e^-}$ may be attainable at FNAL E760, an antiproton accumulator experiment, or at the proposed SuperLEAR facility. This would open the door to precision tests of the proton wavefunction, and set us on the road toward understanding QCD at the amplitude level.

## ACKNOWLEDGMENTS

I would like to thank M. Peskin, G. Sterman, and H. Lu for helpful conversations, and S. Brodsky for invaluable advice.

## APPENDIX A. KINEMATICS AND CONVENTIONS

We computed all amplitudes in the center-of-momentum frame, with the outgoing proton momentum along the positive $z$-axis, and the $y$-axis perpendicular to the scattering plane. That is,

$$
\begin{aligned}
p &= E(1,0,0,1) && \text{proton} \ ; \\
p' &= E(1,0,0,-1) && \text{antiproton} \ ; \\
k &= E(1,\sin\theta,0,\cos\theta) && \text{photon } \gamma_1 \ ; \\
k' &= E(1,-\sin\theta,0,-\cos\theta) && \text{photon } \gamma_2 \, .
\end{aligned}
$$

For the photon polarization vectors, we chose

$$
\epsilon_1(\uparrow) = \tfrac{1}{\sqrt{2}}(\cos\theta, i, -\sin\theta) \ , \qquad \epsilon_1(\downarrow) = \tfrac{1}{\sqrt{2}}(-\cos\theta, i, \sin\theta) \ ;
$$

$$
\epsilon_2(\uparrow) = \tfrac{1}{\sqrt{2}}(\cos\theta, -i, -\sin\theta) \ , \qquad \epsilon_2(\downarrow) = \tfrac{1}{\sqrt{2}}(-\cos\theta, -i, \sin\theta) \ .
$$

We worked in the helicity formalism [22] in which the Dirac matrices are

$$
\gamma^0_\pm = -\mathbf{1} \ , \qquad \gamma^i_\pm = \mp\sigma^i \ .
$$

This yields

$$
\not{p}_+ = \not{p}'_- = -2E \begin{pmatrix} 1 & 0 \\ 0 & 0 \end{pmatrix}, \qquad \not{p}_- = \not{p}'_+ = -2E \begin{pmatrix} 0 & 0 \\ 0 & 1 \end{pmatrix},
$$

$$
\not{k}_+ = \not{k}'_- = -2E \begin{pmatrix} c^2 & sc \\ sc & s^2 \end{pmatrix}, \qquad \not{k}_- = \not{k}'_+ = -2E \begin{pmatrix} s^2 & -sc \\ -sc & c^2 \end{pmatrix},
$$

where $s \equiv \sin(\theta/2)$, $c \equiv \cos(\theta/2)$; the polarization vectors become

$$\epsilon_{1+} = -\epsilon_{1-} = \sqrt{2}\begin{pmatrix} sc\alpha - sc\beta & -c^2\alpha - s^2\beta \\ s^2\alpha + c^2\beta & -sc\alpha + sc\beta \end{pmatrix} ,$$

$$\epsilon_{2+} = -\epsilon_{2-} = \sqrt{2}\begin{pmatrix} sc\gamma - sc\delta & s^2\gamma + c^2\delta \\ -c^2\gamma - s^2\delta & -sc\gamma + sc\delta \end{pmatrix} .$$

For an external quark line, we need a factor $x^{-1/2}u_\pm(xp) = u_\pm(p)$. These spinors are

$$u_+(p) = \sqrt{2E}\ (1 \quad 0)\ , \qquad u_-(p) = \sqrt{2E}\ (0 \quad 1)\ ,$$

for the outgoing quarks, and

$$v_+(p') = \sqrt{2E}\ \begin{pmatrix} 0 \\ 1 \end{pmatrix}\ , \qquad v_-(p') = \sqrt{2E}\ \begin{pmatrix} -1 \\ 0 \end{pmatrix}\ ,$$

for the antiquarks [4]; the subscript denotes the helicity.

We find it convenient to adopt the notation

$$(x_i, y_j) \equiv \left(x_i p + y_j p' - k\right)^2 = -x_i \bar{y}_j\, s^2 - \bar{x}_i y_j\, c^2\ .$$

## APPENDIX B: HARD-SCATTERING AMPLITUDES

The nonzero contributions $\tilde{T}$ to $T_H$ are tabulated here. In each case, we list $\tilde{T}^{(d)}$ for only one of the class of diagrams generated by the symmetries $\mathcal{C}$, $\mathcal{E}$, and $\mathcal{X}$. In obtaining the amplitudes not listed, one must bear in mind that $\mathcal{X}$ interchanges photon helicities and $\mathcal{C}$ reverses them. Parentheses indicate repeated diagrams.

| d<br>$\mathcal{X}$(d) | $\mathcal{E}$(d)<br>$\mathcal{X}\circ\mathcal{E}$(d) | $\mathcal{C}$(d)<br>$\mathcal{X}\circ\mathcal{C}$(d) | $\mathcal{C}\circ\mathcal{E}$(d)<br>$\mathcal{X}\circ\mathcal{C}\circ\mathcal{E}$(d) | $\tilde{T}^{\uparrow\uparrow}_{+-}$ | $\tilde{T}^{\uparrow\downarrow}_{+-}$ | $\tilde{T}^{\downarrow\uparrow}_{+-}$ | $\tilde{T}^{\downarrow\downarrow}_{+-}$ |
|---|---|---|---|---|---|---|---|
| A12<br>A21 | B67<br>B76 | B21<br>B12 | A76<br>A67 | $\frac{c}{s}\frac{1}{\bar{x}_1 y_1}$ | 0 | $\frac{c}{s}\frac{1}{x_1 y_1}$ | 0 |
| A13<br>A31 | B63<br>B36 | B25<br>B52 | A75<br>A57 | $sc\frac{\bar{x}_2}{x_2(x_1,\bar{y}_3)}$ | $sc\frac{1}{(x_1,\bar{y}_3)}$ | $sc\frac{\bar{x}_1\bar{x}_2}{x_1x_2(x_1,\bar{y}_3)}$ | $sc\frac{\bar{x}_1}{x_1(x_1,\bar{y}_3)}$ |
| A14<br>A41 | B64<br>B46 | B24<br>B42 | A74<br>A47 | $-s\frac{x_1}{\bar{x}_1(x_1,\bar{y}_3)}$ | $\frac{c^3}{s}\frac{1}{(x_1,\bar{y}_3)}$ | $-sc\frac{1}{(x_1,\bar{y}_3)}$ | $\frac{c^3}{s}\frac{\bar{x}_1}{x_1(x_1,\bar{y}_3)}$ |
| A16<br>A61 | B61<br>B16 | B27<br>B72 | A72<br>A27 | $-sc\frac{1}{(x_1,\bar{y}_3)}$ | $-\frac{c}{s}\frac{x_2+x_3c^2}{x_3(x_1,\bar{y}_3)}$ | $-sc\frac{\bar{x}_1}{x_1(x_1,\bar{y}_3)}$ | $-\frac{c}{s}\frac{\bar{x}_1(x_2+x_3c^2)}{x_1x_3(x_1,\bar{y}_3)}$ |
| A17<br>A71 | B62<br>B26 | (B26)<br>(B62) | (A71)<br>(A17) | $\frac{c^3}{s}\frac{\bar{y}_3}{y_3(x_1,\bar{y}_3)}$ | $\frac{c^3}{s}\frac{1}{(x_1,\bar{y}_3)}$ | $\frac{c^3}{s}\frac{\bar{x}_1\bar{y}_3}{x_1y_3(x_1,\bar{y}_3)}$ | $\frac{c^3}{s}\frac{\bar{x}_1}{x_1(x_1,\bar{y}_3)}$ |
| A22<br>A2$\bar{2}$ | B77<br>B7$\bar{7}$ | B1$\bar{1}$<br>B11 | A6$\bar{6}$<br>A66 | $-\frac{c}{s}\frac{1-y_1c^2}{\bar{x}_1y_1\bar{y}_1}$ | $-\frac{c^3}{s}\frac{1}{\bar{x}_1\bar{y}_1}$ | $sc\frac{1}{\bar{x}_1\bar{y}_1}$ | $-sc\frac{1}{\bar{x}_1\bar{y}_1}$ |
| A23<br>A32 | B73<br>B37 | B15<br>B51 | A65<br>A56 | $-\frac{s}{c}\frac{\bar{x}_2(y_2+y_1c^2)}{x_2y_1(x_1,\bar{y}_3)}$ | $-\frac{s}{c}\frac{y_2+y_1c^2}{y_1(x_1,\bar{y}_3)}$ | $-\frac{s^3}{c}\frac{\bar{x}_2}{x_2(x_1,\bar{y}_3)}$ | $-\frac{s^3}{c}\frac{1}{(x_1,\bar{y}_3)}$ |
| A24<br>A42 | B74<br>B47 | B14<br>B41 | A64<br>A46 | $\frac{s}{c}\frac{x_1\bar{y}_1s^2+\bar{y}_3c^2}{\bar{x}_1y_1(x_1,\bar{y}_3)}$ | $-sc\frac{\bar{x}_1y_2-x_1y_3}{\bar{x}_1y_1(x_1,\bar{y}_3)}$ | $\frac{s^3}{c}\frac{x_1}{\bar{x}_1(x_1,\bar{y}_3)}$ | $-sc\frac{1}{(x_1,\bar{y}_3)}$ |

Appendix B. Hard-scattering amplitudes (continued)

| d<br>$\mathcal{X}$(d) | $\mathcal{E}$(d)<br>$\mathcal{X}\circ\mathcal{E}$(d) | $\mathcal{C}$(d)<br>$\mathcal{X}\circ\mathcal{C}$(d) | $\mathcal{C}\circ\mathcal{E}$(d)<br>$\mathcal{X}\circ\mathcal{C}\circ\mathcal{E}$(d) | $\tilde{T}^{\uparrow\uparrow}_{+-}$ | $\tilde{T}^{\uparrow\downarrow}_{+-}$ | $\tilde{T}^{\downarrow\uparrow}_{+-}$ | $\tilde{T}^{\downarrow\downarrow}_{+-}$ |
|---|---|---|---|---|---|---|---|
| A25<br>A52 | B75<br>B57 | B13<br>B31 | A63<br>A36 | $-\frac{c}{s}\frac{1}{\bar{x}_1 y_1}$ | $-\frac{c}{s}\frac{\bar{y}_2}{\bar{x}_1 y_1 y_2}$ | 0 | 0 |
| A26<br>A62 | B71<br>B17 | (B17)<br>(B71) | (A62)<br>(A26) | $\frac{s}{c}\frac{y_2+y_1c^2}{y_1(x_1,\bar{y}_3)}$ | $-\frac{s}{c}\frac{x_1y_3-x_2y_2+x_3y_1c^2}{x_3y_1(x_1,\bar{y}_3)}$ | $\frac{s^3}{c}\frac{1}{(x_1,\bar{y}_3)}$ | $\frac{s}{c}\frac{x_2+x_3c^2}{x_3(x_1,\bar{y}_3)}$ |
| A34<br>A43 | B34<br>B43 | B54<br>B45 | A54<br>A45 | $-sc\bar{x}_2x_2(\bar{x}_1,y_3)$ | $\frac{c^3}{s}\frac{\bar{x}_2y_3}{x_2\bar{y}_3(\bar{x}_1,y_3)}$ | $-sc\frac{1}{(\bar{x}_1,y_3)}$ | $\frac{c^3}{s}\frac{y_3}{\bar{y}_3(\bar{x}_1,y_3)}$ |
| A35<br>A53 | B35<br>B53 | (B53)<br>(B35) | (A53)<br>(A35) | $-\frac{c^3}{s}\frac{\bar{x}_2}{x_2(\bar{x}_1,y_3)}$ | $-\frac{c^3}{s}\frac{\bar{x}_2\bar{y}_2}{x_2y_2(\bar{x}_1,y_3)}$ | $-\frac{c^3}{s}\frac{1}{(\bar{x}_1,y_3)}$ | $-\frac{c^3}{s}\frac{\bar{y}_2}{y_2(\bar{x}_1,y_3)}$ |
| A44<br>A4$\bar{4}$ | B44<br>B4$\bar{4}$ | (B4$\bar{4}$)<br>(B44) | (A4$\bar{4}$)<br>(A44) | $sc\frac{x_1c^2+\bar{y}_3s^2}{\bar{x}_1\bar{y}_3(\bar{x}_1,y_3)}$ | $sc^3\frac{\bar{x}_1-y_3}{\bar{x}_1\bar{y}_3(\bar{x}_1,y_3)}$ | $-s^3c\frac{\bar{x}_1-y_3}{\bar{x}_1\bar{y}_3(\bar{x}_1,y_3)}$ | $sc\frac{\bar{x}_1s^2+y_3c^2}{\bar{x}_1\bar{y}_3(\bar{x}_1,y_3)}$ |
| C11<br>C1$\bar{1}$ | D66<br>D6$\bar{6}$ | E2$\bar{2}$<br>E22 | F7$\bar{7}$<br>F77 | $-sc\frac{1}{\bar{x}_1\bar{y}_1}$ | $-\frac{c^3}{s}\frac{1}{\bar{x}_1\bar{y}_1}$ | $sc\frac{1}{\bar{x}_1\bar{y}_1}$ | $-\frac{c}{s}\frac{1-x_1c^2}{x_1\bar{x}_1\bar{y}_1}$ |
| C12<br>C21 | D67<br>D76 | E21<br>E12 | F76<br>F67 | 0 | 0 | $\frac{c}{s}\frac{1}{x_1y_1}$ | $\frac{c}{s}\frac{1}{x_1\bar{y}_1}$ |
| C13<br>C31 | D64<br>D46 | E24<br>E42 | F75<br>F57 | 0 | 0 | $-\frac{s}{c}\frac{\bar{x}_2(s^2-x_2)}{x_1x_2(\bar{x}_2,y_1)}$ | $-\frac{s}{c}\frac{s^2-x_2}{x_1(\bar{x}_2,y_1)}$ |

Appendix B. Hard-scattering amplitudes (continued)

| d<br>$\mathcal{X}$(d) | $\mathcal{E}$(d)<br>$\mathcal{X}\circ\mathcal{E}$(d) | $\mathcal{C}$(d)<br>$\mathcal{X}\circ\mathcal{C}$(d) | $\mathcal{C}\circ\mathcal{E}$(d)<br>$\mathcal{X}\circ\mathcal{C}\circ\mathcal{E}$(d) | $\tilde{T}^{\uparrow\uparrow}_{+-}$ | $\tilde{T}^{\uparrow\downarrow}_{+-}$ | $\tilde{T}^{\downarrow\uparrow}_{+-}$ | $\tilde{T}^{\downarrow\downarrow}_{+-}$ |
|---|---|---|---|---|---|---|---|
| C14<br>C41 | D65<br>D56 | E23<br>E32 | F74<br>F47 | 0 | 0 | $\frac{c}{s}\frac{s^2-x_2}{x_1(\bar{x}_2,y_1)}$ | $-\frac{c}{s}\frac{x_2\bar{y}_2+y_2s^2}{x_1y_2(\bar{x}_2,y_1)}$ |
| C15<br>C51 | D61<br>D16 | E27<br>E72 | F73<br>F37 | 0 | $-\frac{c}{s}\frac{1}{x_3\bar{y}_1}$ | $-\frac{s}{c}\frac{1}{x_1\bar{y}_1}$ | $-\frac{1}{sc}\frac{\bar{x}_3s^2+\bar{x}_1c^2}{x_1x_3\bar{y}_1}$ |
| C16<br>C61 | D62<br>D26 | E26<br>E62 | F72<br>F27 | 0 | 0 | $sc\frac{\bar{x}_2}{x_1\bar{y}_1(\bar{x}_2,y_1)}$ | $sc\frac{x_2}{x_1\bar{y}_1(\bar{x}_2,y_1)}$ |
| C17<br>C71 | D63<br>D36 | E25<br>E52 | F71<br>F17 | 0 | 0 | $-\frac{c}{s}\frac{(s^2-x_2)\bar{y}_3}{x_1y_3(\bar{x}_2,y_1)}$ | $-\frac{c}{s}\frac{s^2-x_2}{x_1(\bar{x}_2,y_1)}$ |
| C25<br>C52 | D71<br>D17 | E17<br>E71 | F63<br>F36 | 0 | $\frac{s}{c}\frac{1}{x_3y_1}$ | 0 | $\frac{s}{c}\frac{1}{x_3\bar{y}_1}$ |
| C35<br>C53 | D41<br>D14 | E47<br>E74 | F53<br>F35 | 0 | $-\frac{c}{s}\frac{\bar{x}_2(c^2-x_2)}{x_2x_3(x_2,\bar{y}_1)}$ | 0 | $-\frac{c}{s}\frac{c^2-x_2}{x_3(x_2,\bar{y}_1)}$ |
| C45<br>C54 | D51<br>D15 | E37<br>E73 | F43<br>F34 | 0 | $\frac{s}{c}\frac{c^2-x_2}{x_3(x_2,\bar{y}_1)}$ | 0 | $-\frac{s}{c}\frac{x_2\bar{y}_2+y_2c^2}{x_3y_2(x_2,\bar{y}_1)}$ |
| C55<br>C5$\bar{5}$ | D11<br>D1$\bar{1}$ | E7$\bar{7}$<br>E77 | F3$\bar{3}$<br>F33 | $sc\frac{1}{\bar{x}_3\bar{y}_1}$ | $\frac{c^3}{s}\frac{1}{\bar{x}_3\bar{y}_1}$ | $-sc\frac{1}{\bar{x}_3\bar{y}_1}$ | $\frac{c}{s}1-x_3c^2x_3\bar{x}_3\bar{y}_1$ |
| C56<br>C65 | D12<br>D21 | E76<br>E67 | F32<br>F23 | 0 | 0 | $-sc\frac{\bar{x}_2}{x_3\bar{y}_1(\bar{x}_2,y_1)}$ | $-sc\frac{x_2}{x_3\bar{y}_1(\bar{x}_2,y_1)}$ |
| C57<br>C75 | D13<br>D31 | E75<br>E57 | F31<br>F13 | 0 | 0 | $\frac{c}{s}\frac{\bar{y}_3(s^2-x_2)}{x_3y_3(\bar{x}_2,y_1)}$ | $\frac{c}{s}\frac{s^2-x_2}{x_3(\bar{x}_2,y_1)}$ |

## REFERENCES


1. G. P. Lepage and S. J. Brodsky, *Phys. Rev.* **D22**, 2157 (1980); S. J. Brodsky and G. P. Lepage, *Phys. Rev.* **D24**, 1808 (1981). For a recent review see S. J. Brodsky, SLAC–PUB–5849 (1992).
2. D. Millers and J. F. Gunion, *Phys. Rev.* **D34**, 2657 (1986).
3. G. R. Farrar *et al.*, *Nucl. Phys.* **B311**, 585 (1989).
4. A. N. Kronfeld and B. Nižić, *Phys. Rev.* **D44**, 3445 (1991).
5. B. Nižić, *Phys . Rev.* **D35**, 80 (1987).
6. V. V. Sudakov, *Sov. Phys.–JETP* **3**, 65 (1956).
7. J. Botts and G. Sterman, *Nucl. Phys.* **B325**, 62 (1989) .
8. H. Li and G. Sterman, ITP–SB–92–10.
9. H. Li, ITP–SB–92–25.
10. V. L. Chernyak and A. R. Zhitnitsky, *Nucl. Phys.* **B246**, 52 (1984).
11. V. L. Chernyak, A. A. Ogloblin and I. R. Zhitnitskií, *Yad. Fiz.* **48**, 841 (1988); *Sov. J. Nucl. Phys.* **48**, 536 (1988).
12. I. D. King and C. T. Sachrajda, *Nucl. Phys.* **B297**, 785 (1987).
13. M. Gari and N. G. Stefanis, *Phys. Lett.* **B175**, 462 (1986); *Phys. Rev.* **D35**, 1074 (1987).
14. This is slightly inaccurate when $q^2 = q_l^2 - q_\perp^2 < 0 < q_l^2$. It depends on the approximation $l_\perp \ll q_\perp$, which fails in the region $|q_\perp + l_\perp| \sim \sqrt{q_l^2}$ when $q_l^2 \simeq q_\perp^2$. However, we use it anyway since the spacelike gluon denominators, like the fermion denominators, do not contain terms like $x_i y_j$; thus the errors induced will be less than those from the neglect of transverse momentum in the fermion propagators.

15. When both gluons carry the transverse hard momentum $q_\perp$, we must use $J_0(\sqrt{|q_\perp||(b_i - b_j) + (b_j - b_k)|})$, reflecting the fact that we take only one angular average, rather than $J_0(\sqrt{|q_\perp||b_i - b)j|})J_0(\sqrt{|q_\perp||b_j - b_k|})$.

16. For timelike gluons, the simple analytic continuation $K_0(bQ) \to K_0(ibQ) = (i\pi/2)\, H_0^{(1)}(bQ)$ of the spacelike propagator, where the imaginary part comes from integrating $k_\perp$ through the singularity at $l_\perp^2 = q_l^2$, must be unphysical. The reason is that in $\gamma\gamma \to p\bar{p}$, the only timelike momentum a gluon can carry is the sum of some subset of the outgoing, onshell quark momenta; thus the region $q_l^2 - l_\perp^2 = q^2 < 0 < q_l^2$ is excluded.

17. A. H. Mueller, *Phys. Rept.* **73**, 237 (1981).

18. G. P. Lepage et al., in *Banff 1981, Proc. Particles and Fields 2.*

19. The immediate effect of the scaling might be an factor $\lambda^1$ (as in the long-distance quarkonium potential), but is more likely $\lambda^2$ since the nucleon can be thought of as saturated with a gluon field. In addition, we must account for the increased strength of the running coupling as the transverse momentum scale decreases. This effect, if approximated by a power-law factor, seems to contribute roughly an additional $\lambda^1$.

20. The GS model is distinguished by pronounced asymmetry; this has been criticized by V. L. Chernyak, A. A. Ogloblin and I. R. Zhitnitskiĭ, *Z. Phys.* **C42**, 583 (1989).

21. FNAL E760 Collaboration, FNAL–PUB–92/244–E, submitted to Phys. Rev. Lett.

22. R. Baldini, private communication.

23. G. R. Farrar and F. Neri, *Phys. Lett.* **130B**, 109 (1983).